

Anchored advected interfaces, Oslo model, and roughness at depinning

Assaf Shapira^{1,*} and Kay Jörg Wiese²

¹ Université Paris Cité, CNRS, MAP5, 75006 Paris, France

² CNRS-Laboratoire de Physique de l'Ecole Normale Supérieure, PSL Research University, Sorbonne Université, Université Paris Cité, 24 rue Lhomond, 75005 Paris, France

E-mail: assaf.shapira@normalesup.org

Received 14 March 2023

Accepted for publication 30 April 2023

Published 6 June 2023



Online at stacks.iop.org/JSTAT/2023/063202

<https://doi.org/10.1088/1742-5468/acd2bb>

Abstract. There is a plethora of one-dimensional advected systems with an absorbing boundary: the Toom model of anchored interfaces, the directed exclusion process where in addition to diffusion particles and holes can jump over their right neighbour, simple diffusion with advection, and Oslo sandpiles. All these models share a roughness exponent of $\zeta = 1/4$, while the dynamic exponent z varies, depending on the observable. We show that for the first three models $z = 1$, $z = 2$, and $z = 1/2$ are realized, depending on the observable. The Oslo model is apart with a conjectured dynamic exponent of $z = 10/7$. Since the height in the latter is the gradient of the position of a disordered elastic string, this shows that $\zeta = 5/4$ for a driven elastic string at depinning.

Supplementary material for this article is available [online](#)

Keywords: depinning, roughness exponent, Oslo model, Toom model, anchored advected interface

* Author to whom any correspondence should be addressed.

Contents

1. Introduction	3
2. Models in the aaEW and aaKPZ universality classes	4
2.1. The DEP	4
2.2. Toom's interface model	5
2.3. Continuum theory	6
2.4. Continuum limit of the DEP	6
3. Particle-hole symmetric case—the aaEW universality class	8
3.1. Periodic BC versus anchored interface	8
3.2. Bulk behaviour	8
3.3. Edge behaviour	8
3.4. Basic formulas	9
3.5. Analytic result for the variance of the height	9
3.6. Approximate calculation for large x	11
3.7. Decay of the auto-correlation function	11
3.8. Dynamic exponents $z = 2$, $z = 1$ and $z = 1/2$	13
3.9. Numerical verification	13
3.10. Discrete argument	15
4. Asymmetric case—the aaKPZ universality class	16
4.1. Introduction	16
4.2. Protection of the stationary measure	16
5. Oslo model	17
5.1. Definition	17
5.2. Phenomenology of the Oslo model	19
5.3. Why is $\zeta = \frac{1}{4}$ in the Oslo model?	19
5.3.1. Local time and global time	19
5.3.2. Hydrodynamic behaviour during the lifetime of an avalanche	20
5.3.3. Comparing the Oslo model with aaEW	20
5.4. Adiabatic versus finite advection in the Oslo model	21
5.5. Oslo and quenched Edwards–Wilkinson	22
6. Conclusion	23
Acknowledgments	23
References	23

1. Introduction

Interfaces subject to quenched disorder describe a variety of physical phenomena [1, 2], such as domain walls in magnets [3–5], contact-line depinning [6], fracture [7, 8], or earthquakes [9]. Two situations have to be distinguished: equilibrium and depinning. Equilibrium designates evaluating the partition function in the limit of a vanishing temperature. Depinning occurs when driving a system adiabatically at zero temperature. While equilibrium is given by the ground state, at depinning the system stops at the first stable configuration, which is distinct from the ground state.

Though many numerical studies exist [10–12], and a field theory was developed [2, 13, 14], only a few exact results are available. A notable exception in equilibrium is the roughness exponent $\zeta_{\text{RB}}^{d=1} = 2/3$ for a $1 + 1$ dimensional directed polymer in random-bond (RB) disorder, itself related to the KPZ universality class [1, 15] with roughness $1/2$ and dynamic exponent $z = 1/\zeta_{\text{RB}}^{d=1} = 3/2$ [16]. For random-field (RF) disorder of a d -dimensional interface in $d + 1$ dimensions in equilibrium, scaling arguments correctly predict $\zeta_{\text{RF}}^d = (4 - d)/3$, which can experimentally be seen even in dimension $d = 0$ [17], where it reduces to the Sinai model [18]³.

At depinning, there is the single random-field universality class, and no analytic result is known, apart from $d = 0$ for which $\zeta_{\text{dep}}^{d=0} = 2^-$ [19]. Based on numerical simulations, it was recently conjectured [12] that a driven one-dimensional string has a roughness exponent of $\zeta_{\text{dep}}^{d=1} = 5/4$. (Overhangs, which we exclude, would reduce ζ [20, 21].) Here we aim at demonstrating $\zeta_{\text{dep}}^{d=1} = 5/4$. A key observation is that if the roughness of the string at depinning is $\zeta_{\text{dep}}^{d=1} = 5/4$, the Oslo model [22, 23], of which the height can be viewed as the gradient of the position of a driven string pulled at one end, has a roughness of $\zeta_{\text{Oslo}}^{d=1} = 1/4$.

There are several one-dimensional systems where a scaling exponent of $1/4$ appears, but this is generally in the temporal domain. E.g. the position in space of a marked monomer on a polymer has autocorrelation $\langle [h(0, t) - h(0, t')]^2 \rangle \sim |t - t'|^{2H}$, with $H = 1/4$. This is obtained from standard scaling arguments as $H = \zeta/z$, with $\zeta = 1/2$ and $z = 2$. If these systems are advected, i.e. $z = 1$, the roughness exponent becomes $\zeta = Hz \rightarrow 1/4$ [24–28].

Here we consider a class of models which allow for a hydrodynamic description equivalent to diffusion of a scalar field $h(x, t)$ combined with advection (drift) away from an absorbing boundary at $x = 0$:

$$\begin{aligned} \partial_t h(x, t) &= D \nabla^2 h(x, t) - \mu \nabla h(x, t) + \sigma \xi(x, t), \\ h(0, t) &= 0, \quad \langle \xi(x, t) \xi(x', t') \rangle = \delta(x - x') \delta(t - t'). \end{aligned} \tag{aaEW}$$

We call it the *anchored advected Edwards–Wilkinson* equation (aaEW), and $-\mu \nabla h(x, t)$ the advection term. While in the bulk the stationary state $h(x, \infty)$ can be obtained from a Brownian motion in the comoving frame, close to the boundary we establish in section 3.5 that $\langle h(x, \infty)^2 \rangle \sim \sqrt{x}$, thus $\zeta = 1/4$.

³ The exponent ζ can be extracted from the scaling with distance, or with the confining potential; the latter remains valid in $d = 0$.

This system possesses three distinct dynamical scaling behaviours, characterized by a dynamical exponent $z = 1$ due to the advection term, $z = 2$ for bulk properties in the comoving frame, and $z = 1/2$ for the decay of the equal-point correlation function (in the steady state),

$$\langle h(x, t) h(x, 0) \rangle = \sqrt{\frac{x}{2\pi}} f(t/x^{1/2}). \quad (1)$$

The function f is obtained analytically in section 3.7.

The model (aaEW) is the proper thermodynamic description for a variety of systems. We give two examples—the directed exclusion process (DEP) (section 2.1) and the Toom interface model (section 2.2). For the Oslo model (section 5) a similar mapping can be constructed, with a crucial difference: The *local time* which sets the clock for an update is advanced by the toppling itself, leading to a different dynamical exponent, conjectured to be $z = 10/7$ [12], thus larger than the corresponding exponent $z = 1$ in aaEW, but smaller than the one for diffusion ($z = 2$). Still, the roughness exponent equals $\zeta = 1/4$, independent of whether one considers bulk or boundary driving. The Oslo model (section 5) achieves this by propagating out from the seed *in both directions*; the seed position effectively acts as an absorbing boundary.

In the derivation of a hydrodynamic description as in equation (aaEW), additional terms may appear,

$$\begin{aligned} \partial_t h(x, t) &= D \nabla^2 h(x, t) - \mu \nabla h(x, t) + \sum_{n \geq 2} \lambda_n [\nabla h(x, t)]^n + \sigma \xi(x, t), \\ h(t, 0) &= 0, \quad \langle \xi(x, t) \xi(x', t') \rangle = \delta(x - x') \delta(t - t'). \end{aligned} \quad (2)$$

The perturbation with λ_2 is the most relevant one, leading to the *anchored advected Kardar–Parisi–Zhang* universality class (aaKPZ) discussed in section 4. If this term is forbidden by symmetry, the next relevant one is λ_3 . It is marginally relevant, and believed to modify the effective parameters in the symmetric case [27], but it cannot change the stationary measure in the bulk (section 4.2).

This paper is organized as follows: In section 2 we introduce models in the aaEW and aaKPZ universality classes, first the DEP (section 2.1), then Toom’s interface model (section 2.2); their hydrodynamic description is obtained in section 2.3. In section 3 we derive analytic results for the aaEW universality class, followed by results for the aaKPZ class in section 4. The Oslo model is treated in section 5.

2. Models in the aaEW and aaKPZ universality classes

2.1. The DEP

Here we introduce a new model, the DEP. This is the simplest model we found that breaks left-right symmetry, equivalent to advection. Depending on whether particle-hole symmetry is unbroken or broken, it belongs to the Edwards–Wilkinson or KPZ class.

In this model, each site $x = 1, 2, \dots$ is either empty or occupied. Particles jump with rate 1 to an empty neighbour as in the simple exclusion process, but an additional

directed transition is introduced, which allows particles to jump over a particle to its right (a jump of length 2) with rate 1, and holes over a hole to the right (a jump of length 2) with rate r . The transitions are

1. $10 \rightarrow 01$ with rate 1,
2. $01 \rightarrow 10$ with rate 1,
3. $110 \rightarrow 011$ with rate 1,
4. $001 \rightarrow 100$ with rate r .

A rate $r=1$ preserves the particle-hole symmetry, while breaking the directional (left-right) symmetry. We refer to this model as the *symmetric* DEP (sDEP). The case $r \neq 1$ is referred to as the *asymmetric* DEP (aDEP), which breaks *both* directional and particle-hole symmetry.

When using periodic boundary conditions, the product measure is stationary. This can be derived from the (non-detailed) balance equation. Then the total particle current $j(\rho)$ is given by

$$j(\rho) = 2 [\rho^2(1 - \rho) - r(1 - \rho)^2\rho] = 2\rho(1 - \rho) [\rho - r(1 - \rho)]. \quad (3)$$

Therefore, $\rho_c = \frac{r}{1+r}$ is the critical density, where the overall current vanishes.

In contrast, we consider a large system with closed boundaries, where no particle current is allowed. This leads to *self-organized criticality*, where particle (or hole) excess will be pushed away to the right. Taking $L \rightarrow \infty$ results in a stationary density $\rho = \rho_c = \frac{r}{1+r}$ in the domain of observation.

2.2. Toom's interface model

Toom's model is the subject of many theoretical and numerical studies [24, 29–33]⁴. As in the DEP, each site is either empty or occupied, but while in the DEP the jump range is either 1 or 2, in Toom's model it is unbounded. More precisely, one chooses a spin i , and exchanges it with the next spin to its right which has the opposite sign. The rates, for any $k \in \mathbb{N}$, are

- (1)_k $\underbrace{1 \dots 1}_k 0 \rightarrow 0 \underbrace{1 \dots 1}_k$ with rate 1,
- (2)_k $\underbrace{0 \dots 0}_k 1 \rightarrow 1 \underbrace{0 \dots 0}_k$ with rate r .

When $r=1$, as in the DEP, the particle-hole symmetry is preserved, and we refer to the model as the *symmetric Toom model* (sToom). When $r \neq 1$ this symmetry is broken, and we refer to the model as the *asymmetric Toom model* (aToom).

In Toom's model with periodic boundary conditions each stationary state is non-interacting, i.e. occupations at different sites are independent. The total particle

⁴ We use the low-noise version of the Toom model [29] introduced in [24].

current is

$$\begin{aligned} j(\rho) &= \rho(1-\rho) + 2\rho^2(1-\rho) + 3\rho^3(1-\rho) + \dots - r[(1-\rho)\rho + 2(1-\rho)^2\rho + \dots] \\ &= \frac{\rho}{1-\rho} - \frac{r(1-\rho)}{\rho}. \end{aligned} \quad (4)$$

This current vanishes at the critical density $\rho_c = \frac{\sqrt{r}}{1+\sqrt{r}}$. As thoroughly discussed in [24], the system with closed boundaries and for $L \rightarrow \infty$ reaches a stationary state with this density at its left end.

2.3. Continuum theory

As suggested in [24, 32], these models can be described using a continuum theory. We define the *height function* $h(x, t)$ as the number of particles between the left boundary (first spin at site 1) and x , minus its expectation. In the continuum limit we expect it to solve a stochastic differential equation of the type

$$\partial_t h(x, t) = c + D\nabla^2 h(x, t) - \mu\nabla h(x, t) + \lambda_2[\nabla h(x, t)]^2 + \lambda_3[\nabla h(x, t)]^3 + \dots + \sigma\xi(x, t). \quad (5)$$

Discarding higher-order terms, we are left with two possible limits: for sDEP and sToom, the particle-hole symmetry forces the equation to stay invariant under the transformation $h \mapsto -h$, hence the first and fourth terms are not allowed ($c = \lambda_2 = 0$), and we are left with the *anchored advected Edwards–Wilkinson* equation

$$\begin{aligned} \partial_t h(x, t) &= D\nabla^2 h(x, t) - \mu\nabla h(x, t) + \sigma\xi(x, t), \\ h(t, 0) &= 0, \quad \langle \xi(x, t)\xi(x', t') \rangle = \delta(x - x')\delta(t - t'). \end{aligned} \quad (\text{aaEW})$$

In aDEP and aToom the constant and quadratic terms are allowed, leading to the *anchored advected KPZ* equation

$$\begin{aligned} \partial_t h(x, t) &= D\nabla^2 h(x, t) - \mu\nabla h(x, t) + \lambda_2[\nabla h(x, t)]^2 + c + \sigma\xi(x, t), \\ h(t, 0) &= 0, \quad \langle \xi(x, t)\xi(x', t') \rangle = \delta(x - x')\delta(t - t'). \end{aligned} \quad (\text{aaKPZ})$$

Since $\langle h(x, t) \rangle = 0$ by construction, the first two terms on the rhs vanish on average, and hence

$$c = -\lambda_2 \langle [\nabla h]^2 \rangle. \quad (6)$$

An additional term with $\lambda_3 \neq 0$ may lead to logarithmic corrections [34].

A direct derivation of this limit for Toom's model appears in [24, 32]. We describe here the derivation for the DEP.

2.4. Continuum limit of the DEP

Let us consider the DEP at the critical density $\rho_c = \frac{r}{1+r}$. Define $\eta(x, t)$ to be 1 if there is a particle at x at time t and 0 otherwise. Then the height function h is defined as $h(x, t) := \sum_{y=1}^x [\eta(y, t) - \rho]$.

During a time period dt , the value of h at x changes when particles jump from the left of x to its right or vice versa:

1. $h(x, t + dt) = h(x, t) - 1$ with probability $p_1 = \eta(x, t)[1 - \eta(t, x + 1)]dt$,
2. $h(x, t + dt) = h(x, t) + 1$ w.p. $p_2 = [1 - \eta(x, t)]\eta(t, x + 1)dt$,
3. $h(x, t + dt) = h(x, t) - 1$ w.p. $p_3 = \eta(x, t)\eta(x + 1, t)[1 - \eta(x + 2, t)]dt$,
4. $h(x, t + dt) = h(x, t) - 1$ w.p. $p_4 = \eta(x - 1, t)\eta(x, t)[1 - \eta(x + 1, t)]dt$,
5. $h(x, t + dt) = h(x, t) + 1$ w.p. $p_5 = r[1 - \eta(x, t)][1 - \eta(x + 1, t)]\eta(x + 2, t)dt$,
6. $h(x, t + dt) = h(x, t) + 1$ w.p. $p_6 = r[1 - \eta(x - 1, t)][1 - \eta(x, t)]\eta(x + 1, t)dt$.

First, we calculate

$$\langle h(x, t + dt) - h(x, t) \rangle = (-p_1 + p_2 - p_3 - p_4 + p_5 + p_6)dt.$$

We separate $\eta(x, t)$ into its average ρ plus fluctuations, $\eta(x, t) = \rho + \nabla h(x, t)$. This yields

$$\langle h(x, t + dt) - h(x, t) \rangle = [D\nabla^2 h(x, t) - \mu\nabla h(x, t) + \lambda_2(\nabla h(x, t))^2 + c]dt, \quad (7)$$

$$D = 1 + 3r - 6r\rho + 3r\rho^2 + 3\rho^2, \quad (8)$$

$$\mu = -6r\rho^2 + 8r\rho - 2r - 6\rho^2 + 4\rho \quad (9)$$

$$\lambda_2 = 6r\rho - 4r + 6\rho - 2. \quad (10)$$

The noise term is obtained from

$$\sigma^2 dt = \left\langle \frac{1}{k} \left[\sum_{x=1}^k h(x, t + dt) - h(x, t) \right]^2 \right\rangle. \quad (11)$$

The reason we take a spatial average is to account for correlations: since each of the transitions (1) and (2) contribute 1 to the sum and transition (3) which is equivalent to (4), and transition (5) which is equivalent to (6), contribute 2, we obtain

$$\left\langle \frac{1}{k} \left(\sum_{x=1}^k h(x, t + dt) - h(x, t) \right)^2 \right\rangle = p_1 + p_2 + 4p_3 + 4p_5. \quad (12)$$

Note that p_4, p_6 are spatial shifts of p_3, p_5 hence we must count them only once. This yields

$$\sigma^2 = 2\rho(1 - \rho)(1 + 2r + 2\rho - 2r\rho). \quad (13)$$

Combining these two equations, we obtain for $\rho = \rho_c = \frac{r}{1+r}$

$$D = \frac{4r+1}{r+1}, \quad \mu = \frac{2r}{r+1}, \quad \lambda_2 = 2(r-1), \quad \sigma^2 = \frac{2r(5r+1)}{(r+1)^3}. \quad (14)$$

This is model (aaEW) when $r=1$ and (aaKPZ) when $r \neq 1$. For the symmetric case this gives

$$D = \frac{5}{2}, \quad \mu = 1, \quad \lambda_2 = 0, \quad \sigma^2 = \frac{3}{2}. \quad (15)$$

3. Particle-hole symmetric case—the aaEW universality class

3.1. Periodic BC versus anchored interface

As discussed for Toom's model and the DEP, models in the advected Edwards–Wilkinson universality class have a stationary measure which depends on the boundary condition. A similar behaviour is observed in the continuum limit. If h is a solution of the diffusion equation (aaEW) with periodic boundary conditions, then $\tilde{h}(x, t) = h(x - \mu t, t)$ solves the non-advected Edwards–Wilkinson equation,

$$\begin{aligned} \partial_t \tilde{h}(x, t) &= \partial_t h(x - \mu t, t) - \mu \nabla h(x - \mu t, t) = D \nabla^2 h(x - \mu t, t) + \sigma \xi(x - \mu t, t) \\ &= D \nabla^2 \tilde{h}(x, t) + \sigma \xi(x, t), \quad \langle \xi(x, t) \xi(x', t') \rangle = \delta(x - x') \delta(t - t'). \end{aligned} \quad (16)$$

(We used that $\xi(x, t)$ and $\xi(x - \mu t, t)$ have the same correlations.) In particular, the stationary state for a periodic system of size L is a Brownian motion with periodic boundary conditions (i.e. a Brownian bridge). For $L \rightarrow \infty$, this change of variables is valid on the entire line $x \in \mathbb{R}$. However, if we consider the half line $x \in [0, \infty)$ with Dirichlet boundary condition $h(0) = 0$ as in equation (aaEW), we cannot define \tilde{h} as above, and the stationary state is *not* a Brownian. This choice of boundary, corresponding to an anchored interface, is the subject of this article.

3.2. Bulk behaviour

When considering portions of the interface far away from the origin, the effect of the boundary becomes negligible, and in particular the stationary state on an interval $[x, x + \Delta x]$ looks like a Brownian motion if $\Delta x \ll x$. This is shown rigorously for Toom's model in [33, 35], and we expect a similar behaviour in all models of this universality class.

3.3. Edge behaviour

As mentioned above, unlike the bulk behaviour, the behaviour of the model near the edge is drastically different from the standard Edwards–Wilkinson universality class [24, 28, 32]. The combination of the Dirichlet boundary and the advection term transfers temporal correlations into special ones. In the following, we derive analytic results for the edge behaviour in the anchored case.

3.4. Basic formulas

We solve the advected diffusion equation with Dirichlet boundary conditions, see also [28]⁵. By simple rescaling we write equation (aaEW) in the form:

$$\begin{aligned}\partial_t h(x, t) &= D \nabla^2 h(x, t) - \mu \nabla h(x, t) + \xi(x, t), & h(x=0, t) &= 0. \\ \langle \xi(x, t) \xi(x', t') \rangle &= \delta(x - x') \delta(t - t').\end{aligned}\quad (17)$$

Equation (17) for $x > 0$ is solved by

$$h(x, t) = \int_{y>0} \int_{t'<t} P^\mu(x, t|y, t') \xi(y, t'). \quad (18)$$

Here

$$\begin{aligned}P_0(x, t) &= \frac{e^{-\frac{x^2}{4Dt}}}{\sqrt{4D\pi t}}, \\ P_0^\mu(x, t) &= P_0(x, t) e^{\frac{\mu x}{2D} - \frac{\mu^2 t}{4D}}, \\ P^\mu(x, t|y, t') &= [P_0(|x - y|, t - t') - P_0(x + y, t - t')] e^{\frac{\mu(x-y)}{2D} - \frac{\mu^2(t-t')}{4D}}.\end{aligned}\quad (19)$$

3.5. Analytic result for the variance of the height

In this section we calculate $\langle h(x, t)^2 \rangle$ analytically. The reader only interested in the large-scale behaviour may skip to the next section.

The roughness exponent ζ is given by the behaviour of $\langle h(x, t)^2 \rangle$ in the steady state,

$$\begin{aligned}\langle h(x, t)^2 \rangle &= \int_{y_1>0} \int_{t_1<t} P^\mu(x, t|y_1, t_1) \int_{y_2>0} \int_{t_2<t} P^\mu(x, t|y_2, t_2) \langle \xi(y_1, t_1) \xi(y_2, t_2) \rangle \\ &= \int_{y>0} \int_{t'<t} P^\mu(x, t|y, t')^2.\end{aligned}\quad (20)$$

This is independent of t , and we will drop t from now on. To proceed, we use the Fourier-transform of the propagator (19),

$$\begin{aligned}P^\mu(x, t|y, 0) &= \frac{e^{-\frac{\mu^2 t}{4D} + \frac{\mu(x-y)}{2D}}}{\sqrt{4D\pi t}} \left[e^{-\frac{(x-y)^2}{4Dt}} - e^{-\frac{(x+y)^2}{4Dt}} \right] \\ &= \int \frac{dk}{2\pi} \left[e^{ik(x-y)} - e^{ik(x+y)} \right] e^{-k^2 Dt - \frac{\mu^2 t}{4D} + \frac{\mu}{2D}(x-y)}.\end{aligned}\quad (21)$$

⁵ In [28] μ has opposite sign, which is equivalent to studying the equation on the negative half line $(-\infty, 0]$.

From now on, we set $\mu = D = 1$. We can recover the full μ , D and σ -dependence by remarking that

$$\langle h(x)^2 \rangle_\mu = \frac{\sigma^2}{\mu} \left\langle h \left(\frac{\mu x}{D}, \frac{\mu^2 t}{D} \right)^2 \right\rangle_{\mu=D=\sigma=1}. \quad (22)$$

Then

$$\int_{y>0} \int_{t>0} P^{\mu=1}(x, t|y, 0)^2 = \int_{k,p} \frac{-16 k p e^{x[1+i(k+p)]}}{[2(k^2 + p^2) + 1][(k-p)^2 + 1][(k+p)^2 + 1]}. \quad (23)$$

Integrating equation (23) over k yields

$$\langle h(x)^2 \rangle_{\mu=1} = \int_{-\infty}^{\infty} \frac{dp}{2\pi i} \frac{16 p e^{-\sqrt{p^2 + \frac{1}{2}}x + i p x}}{(4p^2 + 1)^2}. \quad (24)$$

Equation (24) can be simplified, using for the denominator

$$\int_0^{\infty} dt t e^{-at} = \frac{1}{a^2}, \quad (25)$$

and for $e^{-\sqrt{p^2 + \frac{1}{2}}x}$

$$\int_{s>0} \frac{e^{-as - \frac{1}{4s}}}{2\sqrt{\pi} s^{3/2}} = e^{-\sqrt{a}}. \quad (26)$$

Then the integral over p can be done, leading to

$$\langle h(x)^2 \rangle_{\mu=1} = \int_{s>0} \int_{t>0} \frac{2tx e^{-\frac{x^2}{4sx^2+16t} - \frac{sx^2}{2} - \frac{1}{4s} - t + x}}{\pi s^{3/2}(sx^2 + 4t)^{3/2}}. \quad (27)$$

Setting $s \rightarrow 4st/x^2$, and integrating over t yields

$$\langle h(x)^2 \rangle_{\mu=1} = \int_{s>0} \frac{e^x x^2 K_0 \left(\frac{(2s+1)x}{2\sqrt{s}\sqrt{s+1}} \right)}{4\pi s^{3/2}(s+1)^{3/2}}. \quad (28)$$

K_0 is the Bessel K_0 -function. This can further be simplified, by first setting $y = \sqrt{s/(1+s)}$, and second $2u = y + y^{-1}$. The final result is

$$\langle h(x)^2 \rangle_{\mu=1} = \frac{x^2 e^x}{\pi} \int_1^{\infty} K_0(xu) du = \frac{x e^x}{\pi} \int_x^{\infty} K_0(u) du. \quad (29)$$

The integral is known analytically,

$$\langle h(x)^2 \rangle_{\mu=1} = \frac{x e^x}{2} \left[1 - x (\mathbf{L}_{-1}(x) K_0(x) + \mathbf{L}_0(x) K_1(x)) \right]. \quad (30)$$

The function $\mathbf{L}_n(x)$ is the modified Struve-function. For $\mu \neq 1$ this reads according to equation (22)

$$\langle h(x)^2 \rangle = \frac{x e^{\mu x}}{\pi} \int_{\mu x}^{\infty} K_0(u) du. \quad (31)$$

One can approximate the Bessel function for large argument as

$$K_0(x) = e^{-x} \left[\sqrt{\frac{\pi}{2x}} + \mathcal{O}(x^{-\frac{3}{2}}) \right]. \quad (32)$$

Then the integration can be done analytically,

$$\langle h(x)^2 \rangle \simeq \frac{e^{\mu x} x \operatorname{erfc}(\sqrt{\mu x})}{\sqrt{2}} = \frac{\sqrt{x}}{\sqrt{2\pi\mu}} + \mathcal{O}(x^{-\frac{1}{2}}). \quad (33)$$

This gives a roughness exponent

$$\zeta = \frac{1}{4}. \quad (34)$$

3.6. Approximate calculation for large x

From figure 1 we see that, for large x , we can approximate equation (18) as

$$\begin{aligned} h(x, t=0) &= \int_0^{\infty} dy \int_{-\infty}^0 dt' P^{\mu}(x, t|y, t') \xi(y, t') \\ &\approx \int_{-\infty}^{\infty} dy \int_{-\frac{x}{\mu}}^0 dt' P_0^{\mu}(x-y, -t') \xi(y, t') \\ &= \int_{-\infty}^{\infty} dy \int_0^{\frac{x}{\mu}} dt' P_0^{\mu}(x-y, t') \xi(y, t'). \end{aligned} \quad (35)$$

Then

$$\begin{aligned} \langle h(x)^2 \rangle &\approx \int_{-\infty}^{\infty} dy \int_0^{\frac{x}{\mu}} dt' P_0^{\mu}(x-y, t')^2 \\ &= \frac{1}{\sqrt{8\pi}} \int_0^{\frac{x}{\mu}} \frac{dt'}{\sqrt{t'}} = \sqrt{\frac{x}{2\pi\mu}}. \end{aligned} \quad (36)$$

This reproduces the result of equation (33).

3.7. Decay of the auto-correlation function

We wish to calculate (with $\mu = D = 1$)

$$\langle h(x, t) h(x, 0) \rangle = \int_{y>0} \int_{t'<0} P_{\mu}(x, 0|y, t') P_{\mu}(x, t|y, t'). \quad (37)$$

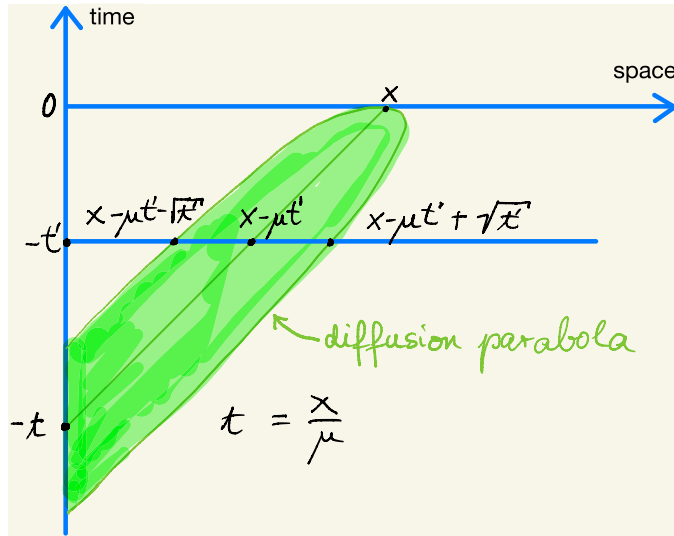


Figure 1. Sketch of the domain contributing to the integral (35). Support in space at given time t' is restricted to the *diffusion parabola* as indicated. This implies that for $0 < t' < t$ the Dirichlet propagator can be approximated by the free propagator, and the space integral extended to ∞ . By the same argument, times $t' > t$ do not contribute.

With the help of equation (35), this can be approximated as

$$\langle h(x, t) h(x, 0) \rangle \approx \int_y \int_{0 \leq t' \leq x} P_0^\mu(y, t') P_0^\mu(y + t, t + t'). \quad (38)$$

Therefore

$$\begin{aligned} \langle h(x, t) h(x, 0) \rangle &\simeq \int_{-\infty}^{\infty} \frac{dk}{2\pi} \int_{-\infty}^{\infty} \frac{dp}{2\pi} \int_y \int_{0 \leq t' \leq x} e^{ik(x-y+t')-k^2 t'} e^{ip(x-y+t+t')-p^2(t+t')} \\ &= \int_{0 \leq t' \leq x} \int_{-\infty}^{\infty} \frac{dk}{2\pi} e^{-k^2(t+2t')-ikt} = \int_{0 \leq t' \leq x} \frac{e^{-\frac{t^2}{4(t+2t')}}}{2\sqrt{\pi}\sqrt{t+2t'}} \\ &= \frac{1}{4} \sqrt{\frac{t}{\pi}} \int_0^{\frac{2x}{t}} dy \frac{e^{-\frac{t}{4(1+y)}}}{\sqrt{1+y}} = \frac{t}{8\sqrt{\pi}} \left[\Gamma\left(-\frac{1}{2}, \frac{t^2}{4(t+2x)}\right) - \Gamma\left(-\frac{1}{2}, \frac{t}{4}\right) \right]. \quad (39) \end{aligned}$$

The Γ -function decays as a power-law corrected Gaussian for large second argument. As we are interested in both large x and large t , the second term vanishes; the first one implies that the proper scaling variable is t/\sqrt{x} , reducing the denominator of the first term from $t + 2x \rightarrow 2x$. As a result,

$$\langle h(x, t) h(x, 0) \rangle \simeq \sqrt{\frac{x}{2\pi}} f\left(\frac{t}{\sqrt{x}}\right), \quad f(0) = 1, \quad f(y) \xrightarrow{y \rightarrow \infty} 0,$$

$$f(y) = \frac{y}{4\sqrt{2}} \Gamma\left(-\frac{1}{2}, \frac{y^2}{8}\right). \quad (40)$$

We tested this against a numerical integration of the exact expression. This worked, but only for large x and t ; for small times our approximation converges from the wrong side. $f(y)$ has series expansions for small and large y

$$\begin{aligned} f(y) &= 1 - \frac{1}{2} \sqrt{\frac{\pi}{2}} y + \frac{y^2}{8} - \frac{y^4}{384} + \frac{y^6}{15360} + \dots \\ f(y) &= e^{-\frac{y^2}{8}} \left[\frac{4}{y^2} - \frac{48}{y^4} + \frac{960}{y^6} + \dots \right]. \end{aligned} \quad (41)$$

Putting back the dependence on μ , D and σ yields with equation (22)

$$\langle h(x, t) h(x, 0) \rangle \simeq \sigma^2 \sqrt{\frac{x}{2\pi\mu D}} f\left(\frac{\mu^2 t}{\sqrt{Dx\mu}}\right). \quad (42)$$

3.8. Dynamic exponents $z = 2$, $z = 1$ and $z = 1/2$

Our calculations above teach us that

$$z = \begin{cases} 2 & \text{for bulk observables in the comoving (advected) frame} \\ 1 & \text{for bulk observables in the fixed frame} \\ \frac{1}{2} & \text{for } \langle h(x, t) h(x, 0) \rangle \end{cases} \quad (43)$$

In particular, we stress that at a time scale $t \sim L$ we reach stationarity on the interval $[0, L]$ (see also [33, 35]).

3.9. Numerical verification

In the symmetric case, we expect the (centred) height function h in both Toom's model and the DEP to converge to the solution of the aaEW equation (aaEW) (up to possible logarithmic corrections). In order to test this, we compare the correlation $\langle h(x, t) h(x, 0) \rangle$ to equation (42).

In figure 2 we show this comparison for Toom's model. It is worth noting, as already mentioned in [24], that there are no finite-size effects in this simulation. We see that the analytic prediction (42) is well verified. (We did not check the dependence on parameters μ , D , and σ). For more thorough numerical studies of this model we refer the reader to [24, 32, 36].)

In figure 3 we show the same plot for the sDEP. There are noticeable finite-size effects, but for large systems the rescaled correlator $\langle h(x, t) h(0, 0) \rangle x^{-1/2}$ plotted against t/x^2 seemingly converges. Remarkably, we obtain not only the correct exponent $\zeta = \frac{1}{4}$, but also the correct coefficient: after rescaling equation (17) to account for the coefficients D and σ in equation (aaEW), and plugging in D, μ and σ found in section 2.4,

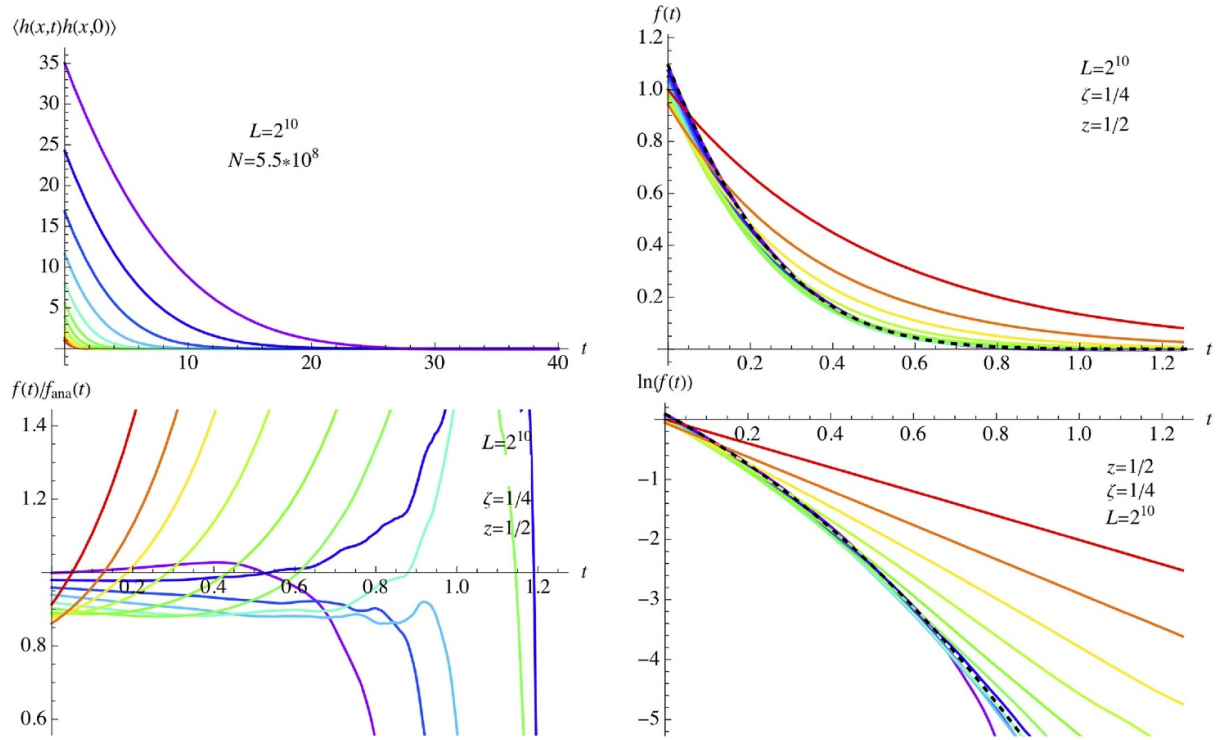


Figure 2. Simulation of the height correlations in the symmetric Toom model of size $L = 2^{10}$, after $N = 5.5 \cdot 10^7$ iterations. (Top left) Height-correlation function for $x = 2$ (small, red), $x = 4$, $x = 8, \dots$ to $x = 2^{10}$ (largest, violet). (Top right) Convergence (same colour code) of the scaling function $f(t)$ against the function of equation (40) (black dashed), with two arbitrary scales. (Bottom left) The ratio of measured $f(t)$ to analytic prediction. (Bottom right) $f(t)$ on a log-scale.

we obtain

$$\langle h(x)^2 \rangle \approx \frac{\sigma^2}{\sqrt{2\pi\mu D}} \sqrt{x} = \sqrt{\frac{9}{20\pi}} \sqrt{x} \approx 0.378 \sqrt{x}.$$

This relation, including the coefficient of 0.378 is verified numerically, as can be seen on figure 3. On the other hand, the rescaling factor for the argument of f is off by a factor of about 1.66,

$$\langle h(x,t)h(0,0) \rangle x^{-1/2} \approx \sqrt{\frac{9}{20\pi}} f \left(1.66 \sqrt{\frac{2}{5}} \frac{t}{\sqrt{x}} \right). \quad (44)$$

This factor, which seemingly affects time scales only, may be due to the presence of sub-sub-leading corrections $\sim (\nabla h)^3$ in the equation of motion. The presence of this type of corrections has been discussed in [34, 36]. As a marginal perturbation $(\nabla h)^3$ gives logarithmic corrections, which may be of the form $\ln L$ or $\ln t$. Our

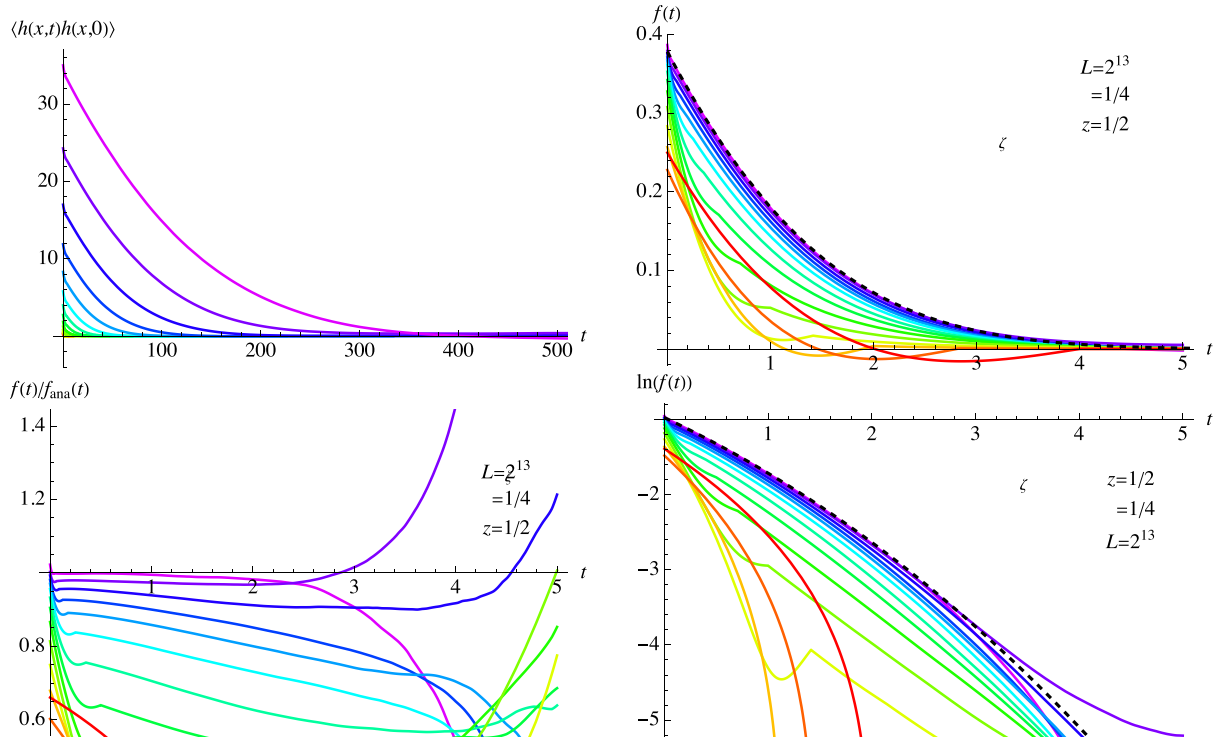


Figure 3. Simulation of sDEP for $L = 2^{13}$, after $N = 5 \cdot 10^{12}$ iterations. (Top left) Height-correlation function for $x = 2$ (small, red), $x = 4$, $x = 8$, ... to $x = 2^{13}$ (largest, violet). (Top right) Convergence (same colour code) of the scaling function $f(t)$ against the function of equation (40) (black dashed), with two fitted scales, and dropping the first data point. The amplitude is as predicted in equation (44). (Bottom left) The ratio of measured $f(t)$ to analytic prediction. (Bottom right) $f(t)$ on a log-scale.

simulation suggests that the combination $\frac{\sigma^2}{\sqrt{\mu D}}$ does not renormalize, while each coefficient by itself may renormalize. In particular the combination μ^3/D renormalizes by a factor of 2.8 at $L = 2^{13}$. We show in section 4.2 that σ^2/D does not renormalize in the bulk. In summary, static observables seem not to renormalize, while temporal correlations do.

The code used to simulate the DEP is available with this paper.

3.10. Discrete argument

The exponent $z = \frac{1}{2}$ in the aaEW universality class can also be derived directly in the discrete model, without passing to the continuum limit.

Consider the height function $h(L)$ of the sDEP at fixed position L . This function only changes when a particle or a hole at L or $L + 1$ jumps to the right of L . Since the density is approximately $1/2$, at any such jump $h(L)$ increases by 1 with probability close to $1/2$ and decreases by 1 with probability close to $1/2$. However, due to density fluctuations, this probability is not exactly $1/2$. When the density is slightly above $1/2$

there are more particles, and h is more likely to decrease. Conversely, when the density fluctuates below $1/2$, it is more likely to increase. The exact correction is complicated, depending on non-trivial correlations, but to first order we may assume that it induces a drift $-\alpha h(L)$ with $\alpha > 0$, possibly L -dependent. We conclude that $h(L)$ behaves as a random walk with a drift term $-\alpha h(L)$, equivalent to diffusion in a confining potential $\frac{\alpha}{2}h(L)^2$. For this process, we know that $h(L)$ fluctuates on a scale $\alpha^{-1/2}$ and that its relaxation time is of order $1/\alpha$. Finally, since $\zeta = \frac{1}{4}$, the fluctuations of h are of order $L^{1/4}$. Comparing this scaling with $\alpha^{-1/2}$ suggests that α scales as $L^{-1/2}$, and hence $z = \frac{1}{2}$.

4. Asymmetric case—the aaKPZ universality class

4.1. Introduction

The aaKPZ universality class can be analysed in a similar manner. As in the symmetric case, the stationary state in the periodic or infinite system is that of Brownian motion, and the bulk behaviour is determined by the KPZ equation in the comoving frame. The edge behaviour in the aaKPZ universality class can then be studied using methods close to those described above [24–27], yielding a roughness exponent $\zeta = \frac{1}{3}$, and dynamical exponents $z = \frac{3}{2}$ for bulk observables in the comoving frame, $z = 1$ for bulk observables in the fixed frame, and $z = \frac{2}{3}$ for $\langle h(x, t)h(x, 0) \rangle$.

4.2. Protection of the stationary measure

Consider the equation of motion (17), with a subleading KPZ-term, and a subsubleading term $\sim (\nabla h)^3$,⁶

$$\eta \partial_t h(x, t) = D \nabla^2 h(x, t) - \mu \nabla h(x, t) + \lambda_2 [\nabla h(x, t)]^2 + \lambda_3 [\nabla h(x, t)]^3 + \cdots + \xi(x, t). \quad (45)$$

In the absence of boundaries, the measure $\mathcal{P}_t[h]$ satisfies the Fokker–Planck equation

$$\eta \partial_t \mathcal{P}_t[h] = \sigma^2 \int_x \frac{\delta^2}{\delta h(x)^2} \mathcal{P}_t[h] - \int_x \frac{\delta}{\delta h(x)} \left\{ \left(D \nabla^2 h(x) - \mu \nabla h(x, t) + \sum_{n \geq 2} \lambda_n [\nabla h(x)]^n \right) \mathcal{P}_t[h] \right\}. \quad (46)$$

Similar to what happens for KPZ, (see e.g. [2], section 7.12), for $\mu = \lambda_i = 0$, a steady-state solution $\partial_t \mathcal{P}^{\text{ss}}[h] = 0$ can be found by asking that

$$\sigma^2 \frac{\delta}{\delta h(x)} \mathcal{P}^{\text{ss}}[h] = D \nabla^2 h(x) \mathcal{P}^{\text{ss}}[h]. \quad (47)$$

⁶ Here we extend an argument initially given for the KPZ equation. While it may be well known in this more general form, we could not find a reference in the literature. J. Krug mentions it in his Diplomarbeit of 1985 at Munich university.

This is solved by

$$\mathcal{P}^{\text{ss}}[h] = \mathcal{N} \exp \left(-\frac{\sigma^2}{2D} \int_x [\nabla h(x)]^2 \right). \quad (48)$$

What is the effect of the additional terms? Inserting the steady state into equation (46) yields

$$\begin{aligned} \eta \partial_t \mathcal{P}^{\text{ss}}[h] &= - \int_x \frac{\delta}{\delta h(x)} \left\{ \left(-\mu \nabla h(x, t) + \sum_{n \geq 2} \lambda_n [\nabla h(x)]^n \right) \mathcal{P}^{\text{ss}}[h] \right\} \\ &= \frac{\sigma^2}{D} \int_x \nabla^2 h(x) \left(-\mu \nabla h(x, t) + \sum_{n \geq 2} \lambda_n [\nabla h(x)]^n \right) \mathcal{P}^{\text{ss}}[h] \\ &= \frac{\sigma^2}{D} \int_x \nabla \left(-\frac{\mu}{2} [\nabla h(x, t)]^2 + \sum_{n \geq 2} \frac{\lambda_n}{n+1} [\nabla h(x)]^{n+1} \right) \mathcal{P}^{\text{ss}}[h] = 0. \end{aligned} \quad (49)$$

Note that by going from the first to the second line, we have dropped the derivative of the terms inside the big round brackets, since they are a total derivative. The last line vanishes, again due to the fact that this is a total derivative.

This calculation shows that as long as we consider a system without boundaries, the steady state is independent of μ and λ_n . When we consider the system from an RG perspective, this means that σ^2/D is not renormalized. There is nothing, however, to protect η/D . In the presence of a boundary, we do not expect bulk properties to renormalize differently, thus the effective η , D , μ , and λ_i to be unchanged if a boundary is introduced.

Let us mention, that from an RG perspective there may appear additional renormalizations on the boundary, and since $\langle h(x, t) h(x, 0) \rangle$ depends on the distance x to the boundary, they could appear there. Since the static 2-point function $\langle h(x, t)^2 \rangle$ shows no corrections, and temporal-derivative terms are marginal in the bulk, we do not expect this to be the case. It would be interesting to render this intuitive argument more rigorously.

5. Oslo model

5.1. Definition

The Oslo model describes the evolution of a sand pile, given by its height h (number of grains) at each horizontal position (see figure 4). In a real sandpile, whether a grain at site i slides downhill depends on the local slope $z(i)$, the friction with its neighbours of contact, and its orientation. The Oslo model is a simple one-dimensional model for this phenomenon, which depends only on the local slope $z(i)$, and a random variable $z_c(i)$. It was introduced in [22, 23], and is defined as follows: Consider the height function $h(i)$ in the left of figure 4. To each height profile $h(i)$ associate a stress field (slope) $z(i)$ defined by

$$z(i) := h(i) - h(i+1). \quad (50)$$

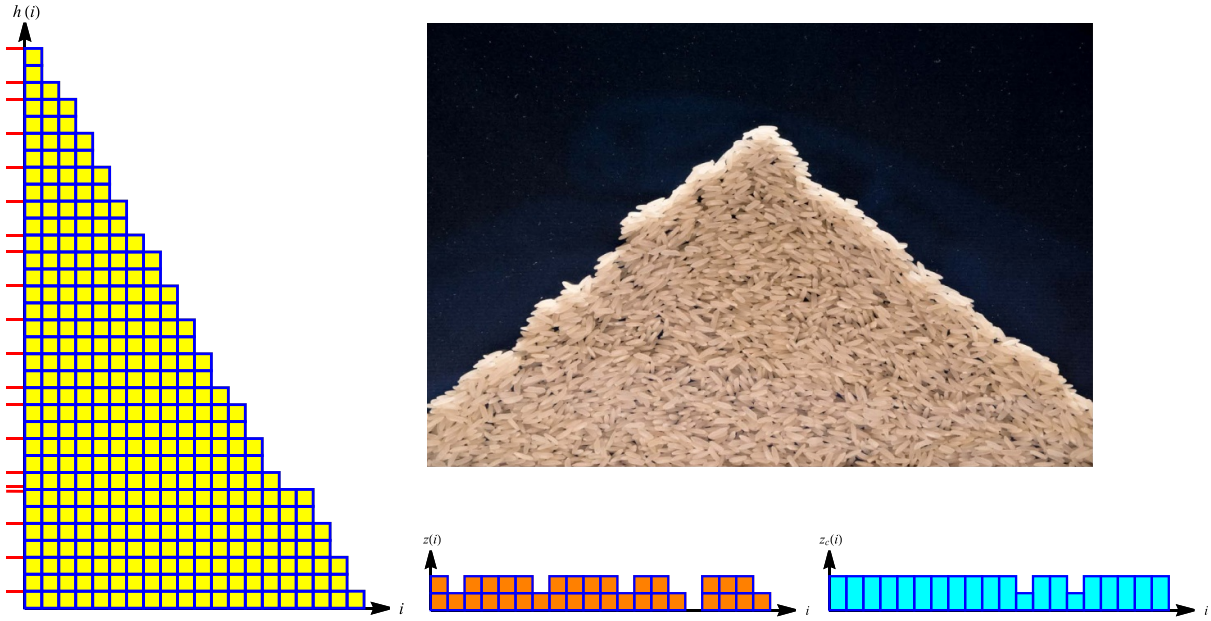


Figure 4. (Left) A stable configuration of the Oslo model. The latter is a cellular automaton version of the right half of the rice pile at the top. (Middle bottom) The variable z defined in equation (50). (Right) The critical value of z for the stable configuration in the middle.

In addition, at each position there is a threshold $z_c(i)$. A toppling is invoked if $z(i) > z_c(i)$, $i > 1$. The toppling rules are

$$z(i) \rightarrow z(i) - 2, \quad z(i \pm 1) \rightarrow z(i \pm 1) + 1. \quad (51)$$

They can be interpreted as moving a grain from the top of the column at site i to the top of the column at site $i + 1$,

$$h(i) \rightarrow h(i) - 1, \quad h(i + 1) \rightarrow h(i + 1) + 1. \quad (52)$$

After such a move, the threshold $z_c(i)$ for site i is updated,

$$z_c(i) \rightarrow \text{new random number}. \quad (53)$$

In its original version, the random number is 1 or 2 with probability $1/2$. To obtain figure 4 we used a random number drawn uniformly from the interval $[0, 2]$. This reduces the critical slope.

In this article we consider a system of size L with absorbing (Dirichlet) boundary conditions on the left boundary (site 1) and free (Neumann) boundary conditions on the right boundary (site L). That is, in the h variable, a toppling at 1 happens when $z(1) > z_c(1)$, and it moves a grain from site 1 to site 2. On the right boundary, a toppling at L happens when $h(L) > z_c(L)$, and it removes one grain from h . We can formulate this in the language of the z variables: when a toppling at 1 occurs, $z(1)$ decreases by 2 and $z(2)$ increases by 1 (i.e. the particle that should have gone

to the left exits the system). When a toppling at L occurs, $z(L)$ decreases by 1 and $z(L-1)$ increases by 1 (i.e. the particle that should have gone to the right stays at L).

For further reading on the Oslo model, we refer to [12, 37–41].

5.2. Phenomenology of the Oslo model

Assume that we start with a system containing many grains. Thanks to the Dirichlet boundary condition for h to the right, the system loses grains (h -particles) there until it reaches a critical slope. This critical slope is equivalent to a critical density of z -particles, which leave the system at the left⁷. We note here that sites with no z -particles or a single z -particle are always stable, sites with two z -particles could be stable or unstable, and particles with three or more z -particles are always unstable. This means that the critical slope must be between 1 and 2 (in fact, it equals approximately 1.8).

An important feature of the Oslo model is that it is Abelian (commutative). In our definition we explained which topplings are invoked, but we did not mention the order in which they occur. It is not difficult to see that the final configuration, after all topplings, does not depend on this order: $z(i)$ is given by the number of incoming particles (the topplings at $i-1$ and $i+1$) and the number of outgoing particles (twice the topplings at i). Since a toppling at one site cannot render another site inactive, the total number of topplings at each site does not depend on the order, hence the final configuration also does not depend on the order.

Thanks to the Abelianity of the model, we are allowed to choose freely the order of topplings. To compare the Oslo model with the models presented above, we choose the same type of dynamics, making each site topple with rate 1 if $z(i) > z_c(i)$.

The Oslo model has been studied extensively, and impressively accurate simulations of its critical exponents are known [12]. For the sake of this paper we wish to mention two of these exponents. First, the roughness exponent is conjectured [12] to be $\zeta = \frac{1}{4}$, that is, $\langle [h(i) - h(j)]^2 \rangle \sim |i - j|^{2\zeta}$. In the language of the z -particles, this is a hyperuniform state [42], i.e. the number of particles between i and j fluctuates as $|i - j|^\zeta \ll |i - j|^{1/2}$. The second relevant exponent is the dynamic exponent z_{Oslo} , conjectured [12] to be $z_{\text{Oslo}} = \frac{10}{7}$.

5.3. Why is $\zeta = \frac{1}{4}$ in the Oslo model?

5.3.1. Local time and global time. The quenched noise of the Oslo model may be thought of as a local time shift: z_c is only updated after a toppling, while an annealed version would update z_c at a fixed rate. We therefore define the *local time* at a site x as the number of toppling events at x . This delays the topplings as compared to the models discussed in section 3, but when the topplings occur, their dynamics is faster, so as to ‘catch up’. As a result, we expect the dynamical critical exponent z to be smaller than 2, and indeed $z_{\text{Oslo}} \approx \frac{10}{7} < 2$.

⁷ Note that since due to equation (50) z is the derivative of h . Thus Neumann boundary conditions for h are Dirichlet boundary conditions for z , and vice versa.

5.3.2. Hydrodynamic behaviour during the lifetime of an avalanche. A key observation for the Oslo model is that, during an avalanche, the local time and the global time propagate approximately at the same rate. Therefore, as long as we are interested in the evolution of an avalanche at times which are much shorter than its survival time, we may replace the quenched noise with an annealed one.

5.3.3. Comparing the Oslo model with aaEW. As discussed in the previous section, we consider time scales much shorter than the lifetime of an avalanche. We can therefore assume that the system evolves according to a hydrodynamic limit of the type in equation (5), with an anchored boundary (at the left). In this model, the analogue of the particles in the DEP or the Toom model are the stress variables z .

Unlike the DEP or Toom's model, in the Oslo model not only the number of z -particles is conserved but also their center of mass, i.e.

$$\partial_t \int_w^y h(x, t) dx = \text{topplings at } w - \text{topplings at } y. \quad (54)$$

Let us consider each of the terms in equation (5): The diffusion term $D\nabla^2 h$ and the advection term $\mu\nabla h$ integrate to

$$\int_w^y dx D\nabla^2 h(x, t) = D[\nabla h(y, t) - \nabla h(w, t)], \quad (55)$$

$$\int_w^y dx \mu\nabla h(x, t) = \mu[h(y, t) - h(w, t)], \quad (56)$$

both bounded uniformly in the interval length $y - w$ (i.e. they remain bounded even if $y - w$ becomes large). The quadratic and constant terms are given by

$$\int_w^y dx [\lambda_2 \nabla(h(x, t))^2 + c] \quad (57)$$

The zero-current condition (6) implies that this term vanishes on average. However its fluctuations grow with $y - w$, so it cannot be bounded uniformly. This means that $\lambda_2 = 0$. The cubic term

$$\int_w^y dx \lambda_3 [\nabla h(x, t)]^3 \quad (58)$$

is also a fluctuating term which cannot be bounded uniformly, unless $\lambda_3 = 0$. In summary, the conservation of the center of mass forces $\partial_t h(x, t)$ to be a total derivatives, which is a stronger constraint than the particle-hole symmetry in Toom or the DEP⁸.

The argument above tells us that, for times shorter than $L^{z_{\text{Oslo}}}$, the Oslo model has an aaEW behaviour. Since $z_{\text{Oslo}} > z_{\text{aaEW}} = 1$, we are allowed to consider the model up

⁸ We already point out that this is related to the fact that $h(x, t)$ can be thought of as the gradient of a field $u(x, t)$, see equation (62).

Anchored advected interfaces, Oslo model, and roughness at depinning

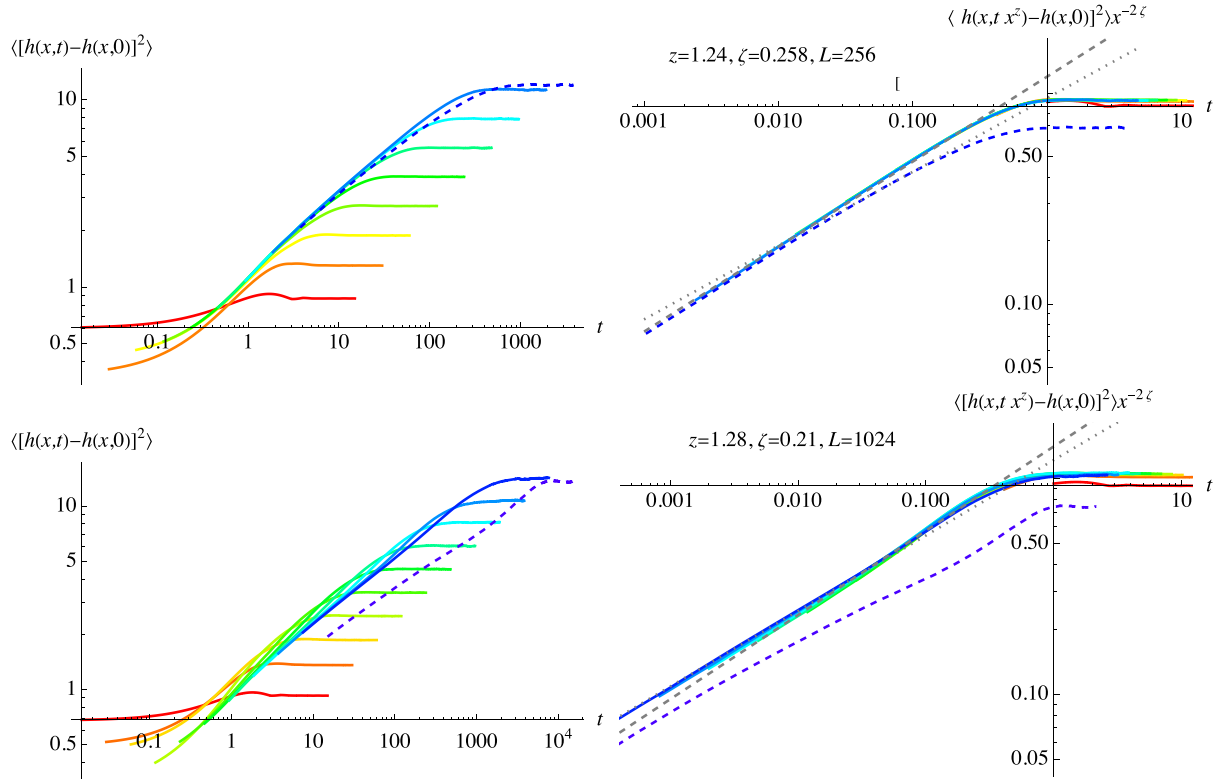


Figure 5. (Top line) The Oslo model at driving rate $r=0$, $L=256$, $x=1, 2, 4, \dots, 256$ (from red over yellow, green, cyan, blue to violet). The last point is at $x=L$, drawn in dashed. It behaves differently from bulk points. The dashed gray line has power $2\zeta/z$ with best-fit values as indicated; the dotted line corresponds to the theoretical prediction $2\zeta/z = 7/20$ ($\zeta = 1/4$, $z = 10/7$). (Bottom line) *ibid* with driving rate $r = 1/5$, and $L = 1024$. See the discussion in section 5.4.

to times $L^{z_{\text{aaEW}}}$. By then the surface reaches a roughness of $\zeta_{\text{aaEW}} = \frac{1}{4}$, which remains the roughness of the Oslo surface.

5.4. Adiabatic versus finite advection in the Oslo model

In figure 5 we show the auto-correlation function in the Oslo model, as a function of ‘grain-time’ t : the protocol is to add one grain, and then to let the full system relax during $n = 1/r$ iterations, or until all sites are stable. As a result, the time t in this simulation is the number of added grains, and r the driving rate. What we measure is the auto-correlation function in the steady state,

$$\langle [h(x,t) - h(x,0)]^2 \rangle \equiv \langle [h(x,t+t') - h(x,t')]^2 \rangle. \quad (59)$$

One observes on figure 5 that for adiabatic driving ($r \rightarrow 0$)

- (i) For each x , it reaches a plateau after some time τ_x . The larger x , the larger τ_x .

- (ii) A scaling collapse can be achieved by the ansatz

$$\left\langle [h(x, t) - h(x, 0)]^2 \right\rangle \simeq x^{2\zeta} f_x(t/x^z) \iff f_x(t) = \left\langle [h(x, tx^z) - h(x, 0)]^2 \right\rangle, \quad (60)$$

where $f_x(t) \rightarrow f(t)$ for $x = 1, 2, 4, \dots, L/2$.

- (iii) The best scaling collapse is achieved by $\zeta = 0.258$ (close to the predicted $\zeta = 1/4$), and $z = 1.24$, definitely smaller than $z = 10/7 = 1.42857$.
- (iv) The last point $x = L$ behaves differently, and its scaling function $f_L(t)$ does not collapse together with the others onto a master curve. While $f_x(t) \sim t^{2\zeta/z}$ with a power given by $\zeta = 0.258$, and $z = 1.24$, the last point has a slope approaching $2\zeta/z = 7/20$.

Let us now turn to a finite driving rate $r = 1/5$, i.e. after adding one grain on the left, we try to topple each site 5 times. Having a finite injection rate, t can both be interpreted as the number of injected grains, or time (divided by 5). We now observe that

- (i) Using the theoretically predicted values of $\zeta = 1/4$ and $z = 10/7$ results in a decent scaling collapse, which improves for larger x .
- (ii) The slope of $f(t)$ in a logarithmic scale does not seem to approach $2\zeta/z$, except for the last point.
- (iii) Things improve for larger system sizes.
- (iv) Remarkably, while we studied smaller driving rates $r = 1/20$ and $r = 1/10$ (not shown) even at the large driving rate of $r = 1/5$ the plots are almost unchanged as compared to $r = 0$, indicating that we are still in a critical state.
- (v) This critical state at large driving can be described by the *anchored advected Edwards–Wilkinson* equation (17).

This confirms our findings that the roughness $\zeta = 1/4$ in the Oslo model has the same origin as in the anchored Edwards–Wilkinson equation (aaEW).

5.5. Oslo and quenched Edwards–Wilkinson

Here we give the relation to depinning in the Edwards–Wilkinson model, of a string of size L [2, 12, 22, 23]. The latter has an equation of motion,

$$\partial_t u(i, t) = \nabla^2 u(i, t) + F(i, u(i, t)), \quad (61)$$

which we read discretized in time t and space i (∇^2 is the discrete Laplacian w.r.t. the variable i). The *random forces* $F(i, u)$ are uncorrelated Gaussian random variables with unit variance. To connect this to the Oslo sandpile, define

$$u(i) := \sum_{j=i+1}^L h(j) + \#\{\text{grains fallen off at the right end}\}. \quad (62)$$

As a consequence, the discrete Laplacian

$$\nabla^2 u(i) = z(i), \quad (63)$$

and the random force $F(i, u)$ stems from the fact that if $u(i) \rightarrow u(i) + 1$, $F(i, u) \rightarrow F(i, u + 1)$ is a new random variable, which identifies with $z_c(i)$ in the Oslo model. The interpretation is that of a string pulled at site $i = 0$ (its left end), with Neumann boundary conditions (no force) at the right end. Its average profile is parabolic,

$$\langle u(i) \rangle \approx \frac{\langle z \rangle}{2} (L - i)^2 + \#\{\text{grains fallen off at the right}\}. \quad (64)$$

As the disorder is renewed after each displacement, it falls into the random-field universality class of depinning [2]. Since $\nabla u \sim h$, a roughness exponent $\zeta = \frac{1}{4}$ for h is the same as a roughness exponent

$$\zeta_{d=1}^{\text{qEW}} = \frac{5}{4} \quad (65)$$

for u . This is what we wanted to show.

6. Conclusion

As we have shown, there is a large class of models which have a roughness exponent of $\zeta = 1/4$. This encompasses the Toom model, advected diffusion with an absorbing boundary, the sDEP, and the Oslo model. Observing that the height in the Oslo model corresponds to the slope of the height in the quenched Edwards–Wilkinson model, we showed that the roughness exponent of the latter is $\zeta_{\text{qEW}} = 5/4$. This puts onto a firm basis the recent conjecture [12] that the numerically observed exponent of $\zeta_{d=1}^{\text{qEW}} = 1.25$ [11] is exactly $\zeta_{d=1}^{\text{qEW}} = 5/4$.

While these models have the same roughness exponent, their dynamical exponent z can be quite different, and depend on the observable. We identified z for the first three models, the *anchored advected universality class*, where we observed a dynamical exponent of $z = 2$, $z = 1$ and even $z = 1/2$, depending on the observable. Our correspondence to the Oslo model cannot (yet) provide its dynamic exponent z , conjectured to be $z = 10/7$, since the arguments use both a global and a local time, which are distinct in this case. Given that $z = 10/7$ is again a simple fraction, we hope that an exact argument may be found as well.

Acknowledgments

We are grateful to Joachim Krug for explaining how advection can convert temporal correlations into spatial ones, and for directing us to the relevant literature. We thank Peter Grassberger for a useful exchange.

References

- [1] Kardar M 1998 Nonequilibrium dynamics of interfaces and lines *Phys. Rep.* **301** 85–112
- [2] Wiese K J 2022 Theory and experiments for disordered elastic manifolds, depinning, avalanches and sandpiles *Rep. Prog. Phys.* **85** 086502
- [3] Durin G and Zapperi S 2006 The Barkhausen effect *The Science of Hysteresis* ed G Bertotti and I Mayergoyz (Amsterdam: Elsevier) p 51
- [4] Durin G, Bohn F, Correa M A, Sommer R L, Le Doussal P and Wiese K J 2016 Quantitative scaling of magnetic avalanches *Phys. Rev. Lett.* **117** 087201
- [5] ter Burg C, Bohn F, Durin G, Sommer R L and Wiese K J 2022 Force correlations in disordered magnets *Phys. Rev. Lett.* **129** 107205
- [6] Le Doussal P, Wiese K J, Moulinet S and Rolley E 2009 Height fluctuations of a contact line: a direct measurement of the renormalized disorder correlator *Europhys. Lett.* **87** 56001
- [7] Ramanathan S, Ertas D and Fisher D S 1997 Quasistatic crack propagation in heterogeneous media *Phys. Rev. Lett.* **79** 873–6
- [8] Ponson L, Bonamy D and Bouchaud E 2006 Two-dimensional scaling properties of experimental fracture surfaces *Phys. Rev. Lett.* **96** 035506
- [9] Fisher D S 1998 Collective transport in random media: from superconductors to earthquakes *Phys. Rep.* **301** 113–50
- [10] Rosso A and Krauth W 2001 Origin of the roughness exponent in elastic strings at the depinning threshold *Phys. Rev. Lett.* **87** 187002
- [11] Ferrero E E, Bustingorry S and Kolton A B 2013 Non-steady relaxation and critical exponents at the depinning transition *Phys. Rev. E* **87** 032122
- [12] Grassberger P, Dhar D and Mohanty P K 2016 Oslo model, hyperuniformity and the quenched Edwards–Wilkinson model *Phys. Rev. E* **94** 042314
- [13] Le Doussal P, Wiese K J and Chauve P 2002 2-loop functional renormalization group analysis of the depinning transition *Phys. Rev. B* **66** 174201
- [14] Chauve P, Le Doussal P and Wiese K J 2001 Renormalization of pinned elastic systems: how does it work beyond one loop? *Phys. Rev. Lett.* **86** 1785–8
- [15] Kardar M, Parisi G and Zhang Y-C 1986 Dynamic scaling of growing interfaces *Phys. Rev. Lett.* **56** 889–92
- [16] Kardar M 1987 Replica Bethe ansatz studies of two-dimensional interfaces with quenched random impurities *Nucl. Phys. B* **290** 582–602
- [17] ter Burg C, Rissone P, Rico-Pasto M, Ritort F and Wiese K J 2023 Experimental test of Sinai’s model in DNA unzipping *Phys. Rev. Lett.* **130** 208401
- [18] Sinai Y G 1983 The limiting behaviour of a one-dimensional random walk in a random environments *Theory Probab. Appl.* **27** 256–68
- [19] Le Doussal P and Wiese K J 2009 Driven particle in a random landscape: disorder correlator, avalanche distribution and extreme value statistics of records *Phys. Rev. E* **79** 051105
- [20] Grassberger P 2018 Universality of critically pinned interfaces in two-dimensional isotropic random media *Phys. Rev. Lett.* **120** 200605
- [21] Grassberger P 2020 Morphological transitions in supercritical generalized percolation and moving interfaces in media with frozen randomness *Phys. Rev. Res.* **2** 043150
- [22] Frette V 1993 Sandpile models with dynamically varying critical slopes *Phys. Rev. Lett.* **70** 2762–5
- [23] Christensen K, Corral A, Frette V, Feder J and Jøssang T 1996 Tracer dispersion in a self-organized critical system *Phys. Rev. Lett.* **77** 107–10
- [24] Derrida B, Lebowitz J L, Speer E R and Spohn H 1991 Dynamics of an anchored Toom interface *J. Phys. A: Math. Gen.* **24** 4805–34
- [25] Krug J, Socolar J E S and Grinstein G 1992 Surface fluctuations and criticality in a class of one-dimensional sandpile models *Phys. Rev. A* **46** R4479–82
- [26] Krug J and Socolar J E S 1992 Comment on “Scalings of growing self-organized surfaces” *Phys. Rev. Lett.* **68** 722
- [27] Krug J 1997 Origins of scale invariance in growth processes *Adv. Phys.* **46** 139–282
- [28] Pruessner G 2004 Drift causes anomalous exponents in growth processes *Phys. Rev. Lett.* **92** 246101
- [29] Toom A L 1980 Stable and attractive trajectories in multicomponent systems *Multicomponent Random Systems* ed R L Dobrushin and Y G Sinai (New York: Marcel Dekker)
- [30] Toom A, Vasilyev N, Stavskaya O, Mityushin L, Kurdyumov G and Pirogov S 1990 *Discrete Local Markov Systems* (Manchester: Manchester University Press)

- [31] Barabási A-L, Araujo M and Stanley H E 1992 Three-dimensional Toom model: connection to the anisotropic Kardar–Parisi–Zhang equation *Phys. Rev. Lett.* **68** 3729–32
- [32] Barkema G T, Ferrari P L, Lebowitz J L and Spohn H 2014 Kardar–Parisi–Zhang universality class and the anchored Toom interface *Phys. Rev. E* **90** 042116
- [33] Crawford N and Kozma G 2020 The Toom interface via coupling *J. Stat. Phys.* **179** 408–47
- [34] Paczuski M, Barma M, Majumdar S N and Hwa T 1992 Fluctuations of a nonequilibrium interface *Phys. Rev. Lett.* **69** 2735
- [35] Crawford N, Kozma G and de Roeck W 2015 The Toom interface via coupling (arXiv:1501.04746)
- [36] Subramanian B, Barkema G T, Lebowitz J L and Speer E R 1996 Numerical study of a non-equilibrium interface model *J. Phys. A: Math. Gen.* **29** 7475
- [37] Dhar D 2004 Steady state and relaxation spectrum of the Oslo rice-pile model *Physica A* **340** 535–43
- [38] Huynh H N, Pruessner G and Chew L Y 2011 The Abelian Manna model on various lattices in one and two dimensions *J. Stat. Mech.* P 09024
- [39] Hinrichsen H 2000 Non-equilibrium critical phenomena and phase transitions into absorbing states *Adv. Phys.* **49** 815–958
- [40] Henkel M, Hinrichsen H and Lübeck S 2008 *Non-Equilibrium Phase Transitions* (Dordrecht: Springer)
- [41] Pruessner G 2012 *Self-Organised Criticality: Theory, Models and Characterisation* (Cambridge: Cambridge University Press)
- [42] Hexner D and Levine D 2015 Hyperuniformity of critical absorbing states *Phys. Rev. Lett.* **114** 110602